Lasers in Surgery and Medicine 44:310–317 (2012)

Narrow Band Imaging of Squamous Cell Carcinoma Tumors Using Topically Delivered Anti-EGFR Antibody Conjugated Gold Nanorods

Priyaveena Puvanakrishnan, PhD,[1*] Parmeswaran Diagaradjane, PhD,[2] S.M. Shams Kazmi,[1] Andrew K. Dunn, PhD,[1] Sunil Krishnan, MD,[2] and James W. Tunnell, PhD[1]

[1]*Department of Biomedical Engineering, The University of Texas at Austin, Austin, Texas 78712*

[2]*Radiation Oncology-Research, The UT MD Anderson Cancer Center, 1515 Holcombe Blvd, Unit-66, Houston, Texas 77030*

Background: Nanoparticles have recently gained interest as exogenous contrast agents in a variety of biomedical applications related to cancer detection and treatment. The objective of this study was to determine the potential of topically administered antibody conjugated gold nanorods (GNRs) for imaging squamous cell carcinomas (SCCs) of the skin using near-infrared narrowband imaging (NBI). Near-infrared (NIR) NBI images narrow wavelength bands to enhance contrast from plasmonic particles in a wide field portable and noncontact device that is clinically compatible for real-time tumor imaging and tumor margin demarcation.

Study design: We conjugated GNRs to Cetuximab, a clinically approved humanized antibody that targets the epidermal growth factor receptor (EGFR), which is overexpressed on the surface of many tumor cells, especially SCCs. We excised subcutaneous xenografts of SCCs (A431) from Swiss *nu/nu* mice and divided the tumors into two groups: (1) the targeted group (Cetuximab conjugated GNRs) and (2) the control group (polyethylene glycol-conjugated GNRs). After topical application of particles and incubation for 30 minutes, the tumors were washed and imaged using NBI. In addition, we performed two-photon imaging to quantify the binding of EGFR targeted GNRs in tumors and their depth profile.

Results: The NBI images showed a visual increase in contrast from tumors after topical administration of targeted GNR. Targeted GNR tumors showed increased contrast compared to tumors administered with the control GNR. There was a statistically significant increase in mean pixel intensity ($\sim$2.5$\times$) from targeted GNR tumors ($n = 6$). Two-photon microscopy images of targeted GNRs confirmed their binding affinity to the EGF receptors over expressed in the A431 tumors.

Conclusion: We have demonstrated that a topical application of gold nanorods targeted specifically to tumor growth factor receptors results in a significantly higher image contrast compared to nontargeted gold nanorods. These results demonstrate the feasibility of near-infrared NBI to image and demarcate tumor margins during surgical resection using topical administration of targeted GNR. Lasers Surg. Med. 44:310–317, 2012.

Key words: gold nanorods; narrow band imaging; epidermal growth factor receptor (EGFR) targeting; two-photon microscopy

INTRODUCTION

Squamous cell carcinoma (SCC) is the second-most common skin cancer after basal cell carcinoma (BCC) with over 250,000 new cases detected every year [1]. However, SCCs are more likely to be aggressive and invade the dermal skin layers. SCCs are typically removed using Mohs surgery that involves sequential removal of small layers of skin followed by examination under the microscope until the samples indicate no residual features of SCC. Mohs surgery requires multiple excisions, with preparation of frozen sections and examination requiring 20–45 minutes per excision [2]. In the case of large SCCs, several excisions may be required, and the total visit time may extend to several hours. Recently, several optical imaging techniques have been developed to enable rapid detection of nonmelanoma skin cancers noninvasively in surgical skin excisions. The techniques include multispectral fluorescence polarization [3,4], confocal reflectance microscopy [2,5,6], optical coherence tomography [7,8] and fluorescence spectroscopy [9]. Several of these imaging methods have utilized extrinsic contrast agents such as acetic acid, methylene blue, and toluidine blue dyes to enhance contrast of the SCC tumor relative to the surrounding normal tissue.

Recently, we combined the advantage of gold nanoshells as exogenous contrast agents along with near-infrared

Conflicts of interest: Priyaveena Puvanakrishnan and James W. Tunnell receive royalties from the University of Texas through a license agreement with Nanospectra Biosciences, Inc.

Contract grant sponsor: National Institutes of Health; Contract grant numbers: R01 CA132032, R21 CA133691; Contract grant sponsor: ASLMS Student Research Grant (2009).

*Corresponding to: Priyaveena Puvanakrishnan, PhD, Department of Biomedical Engineering, The University of Texas at Austin, Austin, TX 78712. E-mail: priyaveena@mail.utexas.edu

Accepted 20 February 2012

Published online 13 March 2012 in Wiley Online Library (wileyonlinelibrary.com).

DOI 10.1002/lsm.22019

© 2012 Wiley Periodicals, Inc.

(NIR) narrow-band imaging for enhanced visualization of tumors [10]. Narrow band imaging (NBI) is a diagnostic technique clinically available today and used in several imaging applications to image morphology near the surface of tissue [11,12]. NBI uses a narrow band of wavelengths matched to the chromophores of interest to highlight contrast between tissue constituents and exogenous contrast agents. Clinical applications of NBI typically exploit contrast of target tissue due to blood by imaging in narrow bands of hemoglobin absorption. In our technique, we image in multiple narrow wavelength bands to exploit two sources of contrast: endogenous (blood) and exogenous (nanorods). We image in the visible and NIR to distinguish between blood and nanorods in the tumor, respectively. In the current study, we have used NBI combined with gold nanorods (GNRs) as contrast agents to image *ex vivo* SCC tumors.

NIR-absorbing GNRs have considerable advantages over molecular dyes and fluorophores as contrast agents for NIR imaging applications. GNRs have tunable optical properties and high optical absorption cross sections in the NIR region, making them attractive probes for *in vitro* and *in vivo* imaging [13,14]. GNRs are stable and their photo-physical properties are much more robust against photobleaching effects [15]. In vivo tumor targeting using GNRs has been achieved using a passive delivery mechanism known as enhanced permeability and retention (EPR) [16]. It has been shown that the nanoparticles when injected systemically or intravascularly, extravasate from the leaky neovasculature and accumulate in tumors due to the EPR effect [17]. In an effort to increase targeting contrast, recent efforts have focused on active targeting strategies, wherein the nanoparticles' surface is functionalized with antibodies to specifically target tumors [18–20]. Loo et al. [20] demonstrated active targeting using anti-HER2 conjugated gold nanoshells to image breast carcinoma cells. El-Sayed et al. have demonstrated active targeting of both nanospheres and nanorods using anti-EGFR antibodies *in vitro* [21,22]. However, even with the systemic delivery of these particles, only a small percentage (~2%) of the administered nanoparticles reach the tumor target [23], and the residual material may raise concerns for toxicity and inadequate clearance from the body.

To reduce the quantity accumulating in vital organs and improve nanoparticle contrast from tumors, we *topically* applied antibody conjugated GNRs on tumor xenograft models and imaged using NBI. Recently, several research groups have used this delivery technique to specifically target disease tissues. Nitin et al. [24] evaluated the fluorescence contrast properties following topical delivery of 2-[*N*-(7-nitrobenz-2-oxa-1,3-diazol-4-yl) amino]-2-deoxy-glucose (2-NBDG) in freshly resected clinical specimens of neoplastic oral mucosa using fluorescence imaging. Bickford et al. used gold nanoshells as rapid diagnostic agents for imaging human breast tissue sections that over-expressed HER2 receptors [25,26].

We targeted the epidermal growth factor receptor (EGFR) over-expressed in SCCs (A431 cancer cells) using GNRs conjugated to Cetuximab (C225, a humanized anti-EGFR antibody that is currently approved for clinical use). EGFR is a transmembrane receptor tyrosine kinase stimulated by growth factors, such as transforming growth factor (TGF)-α or EGF, that binds to the extracellular domain of the receptor [27]. EGFR promotes multiple tumorigenic processes, stimulating proliferation, angiogenesis, and metastasis as well as protecting cells from apoptosis [28]. EGFR is a viable molecular target that has been shown to highly over-express in several skin SCCs [29,30]. Several groups have used EGFR as probes to target, image, and treat A431 cells and tumor xenografts. Durr et al. used anti-EGFR antibody conjugated nanorods to detect and image A431 skin cancer cells embedded in a three-dimensional tissue scaffold using two-photon luminescence (TPL) microscopy [31]. Recently, Melancon et al. [32] used anti-EGFR antibody conjugated hollow gold nanoshells to target A431 cells *in vitro* and *in vivo* and performed photo-thermal ablation of cells *in vitro*.

In this article, we report topical administration of anti-EGFR antibody conjugated GNRs (C225-GNRs) on A431 tumor cross-sections to target EGFR. We imaged the GNRs bound to the SCC tumors using NBI in the NIR region where there is optimal penetration of light through tissue. We imaged the A431 tumor's cross-sections topically administered with both C225-GNRs and pegylated GNRs (control) using NBI. We show that C225-GNRs provided significantly higher tumor contrast compared to non-targeted pegylated GNRs (PEG-GNRs). In addition, we determined the penetration depth of the topically administered C225-GNRs and confirmed their binding affinity in tumors using two-photon microscopy (TPM).

MATERIALS AND METHODS

Synthesis of Pegylated Gold Nanorods (PEG-GNRs)

The nanorods were provided by Nanospectra Biosciences Inc. (Houston, TX). GNRs were synthesized using the method developed by Jana et al. [33]. Briefly, gold seed particles were prepared by adding 250 μl of 10 mM $HAuCl_4{\cdot}3H_2O$ to 7.5 ml of 100 mM CTAB with brief, gentle mixing. 600 μl of freshly prepared, ice-cold 10 mM $NaBH_4$ solution was added and mixed the solution for 2 minutes. The nanorod growth solution was prepared by adding 40 ml of 100 mM CTAB, 1.7 ml of 10 mM $HAuCl_4{\cdot}3H_2O$, and 250 μl of 10 mM $AgNO_3$ followed by 270 μl of 100 mM ascorbic acid. To initiate nanorod growth, 840 μl of the seed solution was added to the growth solution, mixed gently, and left still for 40 minutes. Excess reactants were removed by centrifugation and re-suspension in de-ionized (DI) water. For *in vivo* applications, the GNRs were PEGylated by the addition of 1 mM thiol-terminated methoxypolyethylene glycol (mPEG-SH) (Laysan Bio, Arab, AL) and stirred the solution overnight. The final PEGylated rod solution was cleaned by diafiltration of the solution into DI water. After cleaning, the particles were transferred via diafiltration into a 10% (wt/v) solution of trehalose to make the

solution iso-osmotic with the blood. The GNRs are 24 × 7 nm in size with a strong plasmon resonance peak centered at 776 nm as seen in Figure 1.

Bioconjugation of GNRs to Cetuximab (C225-GNRs)

We adopted a three-step process for the bioconjugation of GNRs to Cetuximab. Our synthesis protocol utilizes the classical thiol-maleimide chemistry and the details of the conjugation process are as follows.

Step-1: Functionalization of GNRs with polyethylene glycol (PEG). Prior to conjugation the CTAB coated GNRs were briefly sonicated to disperse the GNRs into a homogenous suspension. Methoxy-PEG-thiol (monofunctional PEG; mPEG-SH2K) and PEG bis Thiol (bifunctional PEG; SH-PEG5K-SH) were mixed in the ratio of 4:1 to arrive at a final concentration of 2 mM. The freshly made PEG solution was mixed with clean GNRs in the ratio of 1:9, stirred thoroughly and incubated for 1–2 hours at room temperature, with gentle shaking. At the end of the incubation time the GNRs were centrifuged at 10,000 rpm for 20 minutes to remove the unreacted PEG and the pellets were resuspended in PBS to form a uniform suspension of PEG-GNRs, with the terminal thiol (-SH) group at one end of the bifunctional PEG available for further conjugation with antibody.

Step-2: Activation of antibody. Cetuximab® (152 kDa), an anti-epidermal growth factor receptor (EGFR) antibody, is activated by reacting with a heterobifunctional crosslinker, succinimidyl 4-[*N*-maleimidomethyl] cyclohexane-1-carboxylate (SMCC; MW 334.32; arm length 0.83 nm) to expose the maleimide groups for the subsequent conjugation with PEG-GNRs containing free thiol (-SH) moieties. Approximately 20-fold molar excess of SMCC was added to the antibody solution (2 mg/ml) and incubated for 2 hours at 4°C. At the end of the reaction, the unbound cross linker molecules were removed by eluting the reaction mixture through a desalting column and the purified maleimide-activated Cetuximab was collected in a clean tube for further reaction with PEG-GNR.

Step-3: Conjugation of Cetuximab® to GNR. The maleimide-activated Cetuximab (prepared from Step-2) was mixed with the PEG-GNRs with free thiol moieties (prepared from Step-1) such that the final concentration of maleimide-activated Cetuximab is ∼ 10 μg/ml. After overnight reaction at 4°C, the unbound antibody was removed by centrifugation at 9,300 rcf for 20 minutes. The centrifugation step was repeated three times and the pellets were collected and reconstituted in sterile phosphate buffered solution (PBS). The optical density of both PEG-GNRs (plasmon resonance peak @ 776 nm) and C225-GNRs (plasmon resonance peak @ 754 nm) was measured using UV–Vis spectrophotometer (Beckman Coulter DU720, Brea, CA) and their normalized extinction spectra are shown in Figure 1.

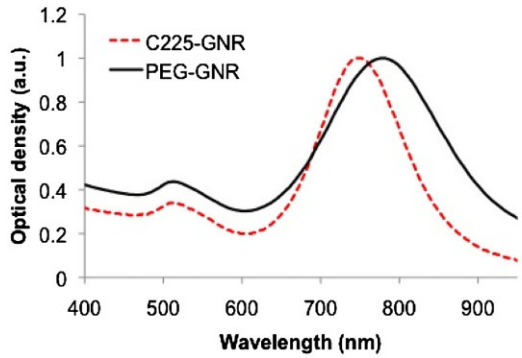

Fig. 1. UV–VIS extinction spectrum of PEG-GNRs and C225-GNRs. [Color figure can be seen in the online version of this article, available at http://wileyonlinelibrary.com/journal/lsm]

The conjugation efficiency was evaluated by measuring the zeta (ζ) potential of the final conjugates. The CTAB coated GNRs used at the beginning of the conjugation process showed a zeta potential in the range +60 to +80 mV. After the functionalization of GNRs with SH-PEG the zeta potential decreased to +5 to +10 mV. With the addition of Cetuximab® to GNRs, the zeta potential further decreased and reached near neutral values in the range of +4 to −5 mV. These values were consistent among different conjugation batches indicating the efficiency of surface functionalization and Cetuximab® conjugation to the surface of GNRs. Finally the conjugation efficiency was validated using a BCA (bicinchoninic acid) protein assay by quantifying the ratio of Cetuximab® to GNR. Prior to the protein estimation the optical density (OD) of PEG-GNRs and C225-GNRs at the assay readout wavelength was adjusted to the same value. PEG-GNRs and C225-GNRs were subjected to assay protocol and the assay end product was measured. With the known values of GNR/ml (2×10^{11} GNR/ml at 1 OD) and the measured concentration of C225 in the C225-GNR samples, the ratio of C225 molecules per GNR was estimated as ∼110–140 C225 molecules/GNR.

Ex Vivo Mouse Skin Tumor Tissues

A431 cells (CRL-1555, ATCC, human epithelial carcinoma cell line) were grown in Dulbecco's Modified Eagle's medium (30–2002, ATCC) with 10% fetal bovine serum (30–2020, ATCC) at 37°C under 5% CO_2. When culture reached 90% confluency, the cells were detached from the flask by 0.25% trypsin–EDTA (30–2101, ATCC), centrifuged, and re-suspended in sterile PBS. Approximately 4×10^6 cells/50 μl were subcutaneously injected in the right thigh of 4–5 week old nude mice (Swiss nu/nu). When tumors attained a size of ∼ 8–10 mm in diameter, we sacrificed the mice and excised the tumors for topical delivery of GNRs followed by imaging. The tumors were frozen immediately after resection and imaged after a month. A whole tumor was sliced vertically into two to expose each cross-section for topical application of PEG-GNRs and C225-GNRs, respectively. We sliced the tissue samples using surgical scissors. We obtained 12 tumor slices from a total of 6 whole tumors to perform topical application of GNRs. The tissue cross-sections were approximately 4 mm thick.

Topical Delivery of PEG-GNRs and C225-GNRs

We performed topical delivery of both PEG-GNRs and C225-GNRs on A431 tumor cross-sections. The tumor sections were divided into the following two groups: (1) Group 1 tumor cross-sections (n = 6) received a topical delivery of 60 μl of PEG-GNRs and was designated the control group; (2) Group 2 tumor cross-sections (n = 6) received 60 μl of C225-GNRs. The optical density of PEG-GNR solution was matched to that of C225-GNR (OD = 25) by diluting in PBS before topically applying on tumors. Because PEG-GNRs have no targeting moiety, they are treated as the control group in our experiments. Prior to nanoparticle delivery baseline NBI images were acquired. Following baseline imaging, the tumor cross-sections were incubated with PEG-GNRs or C225-GNRs for 30 minutes at 37°C under 5% CO_2. At the end of incubation time, the tissues were washed three times with 1× PBS for NBI and two-photon microscopy.

Near-Infrared Narrow Band Imaging

The schematic of the imaging system is shown in Figure 2. The NBI system consists of (1) two light emitting diodes (LED): green (530 nm) and NIR (780 nm) for illuminating the blood vessels and GNRs, respectively; (2) a filter wheel for wavelength selection; and (3) a 12-bit CCD (Basler Pilot, Graftek Imaging, Austin, TX) to collect reflected light from the sample. The filter wheel contains two band pass filters (Semrock, Inc., Rochester, NY), (a) VIS filter (CWL = 536 nm, BW = 40 nm) and (b) NIR filter (CWL = 769 nm, BW = 41 nm) to image the blood vessels and GNRs, respectively. The NBI system is a portable and noncontact device that can perform wide-field, real-time imaging and is clinically compatible for real-time tumor margin demarcation [10].

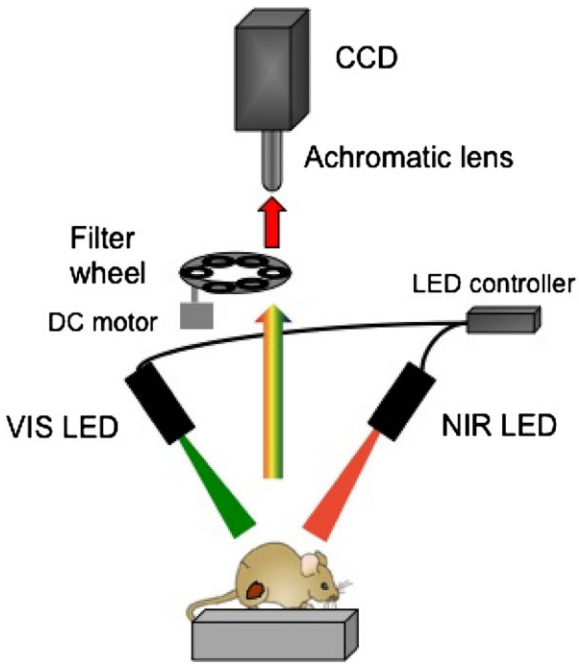

Fig. 2. Schematic of NIR NBI system. [Color figure can be seen in the online version of this article, available at http://wileyonlinelibrary.com/journal/lsm]

Two-Photon Microscopy

We performed two-photon microscopy of the tumor samples incubated with C225-GNRs and PEG-GNRs using a custom-built NIR laser scanning multiphoton microscope described previously [34]. Briefly, we used a femtosecond Ti: Sapphire laser (Mira 900 with excitation wavelength of 800 nm; Coherent, Inc., Santa Clara, CA) as the excitation source, and the laser beam was raster scanned along the sample using a pair of galvanometric scanning mirrors (6215HB; Cambridge Technology, Inc., Lexington, MA) to produce 2D images. We detected the two-photon luminescence from the GNRs using two photomultiplier tubes (PMT) (H7422P-40, H7422P-50; Hammamtsu Corporation, Bridgewater, NJ) through a dichroic beam splitter (FF735-Di01; Semrock, Inc., Rochester, NY). We applied an incident laser power of 40.8 mW and band pass filtering of 6 dB gain. In order to determine the penetration depth of the GNRs, we obtained images (512 × 512 pixels) in the z-direction and created a stack of images to analyze the particle penetration as a function of depth.

RESULTS

NBI of A431 Tumors Topically Administered With PEG-GNRs

Figure 3 presents a qualitative assessment of tumor cross-sections incubated with the control PEG-GNRs. The images show no perceivable contrast in the NIR using NBI. The red color in the NBI images corresponds to blood. We did not observe any PEG-GNRs in the post delivery NIR NBI images after the PBS wash (Fig. 3f).

NBI of A431 Tumors Topically Administered With C225-GNRs

Figure 4 demonstrates that tumors incubated with GNRs targeted specifically to tumor growth factor receptors (bottom row) resulted in a significantly higher image contrast compared to the untargeted tumor (top row). The red color in the NBI images corresponds to blood and the green color corresponds to EGFR-targeted GNRs attached to EGFRs expressed on A431 tumors. The composite NBI images of tumors demonstrated that GNRs targeted specifically to tumor growth factors resulted in higher nanorod binding to tumor receptors and a significantly higher image contrast compared to nontargeted gold nanorods (PEG-GNR). In addition, the NBI images highlight the regions of C225-GNR binding to the tumor receptors compared to the standard color images.

Quantitative Analysis of Tumor Cross Sections Incubated With GNRs

We quantified the image contrast obtained with tumor images from both experimental groups. Prior to topical application of GNRs, there was no significant difference in mean reflectance intensity between C225- and PEG-GNR treated tumors. As seen in the images from

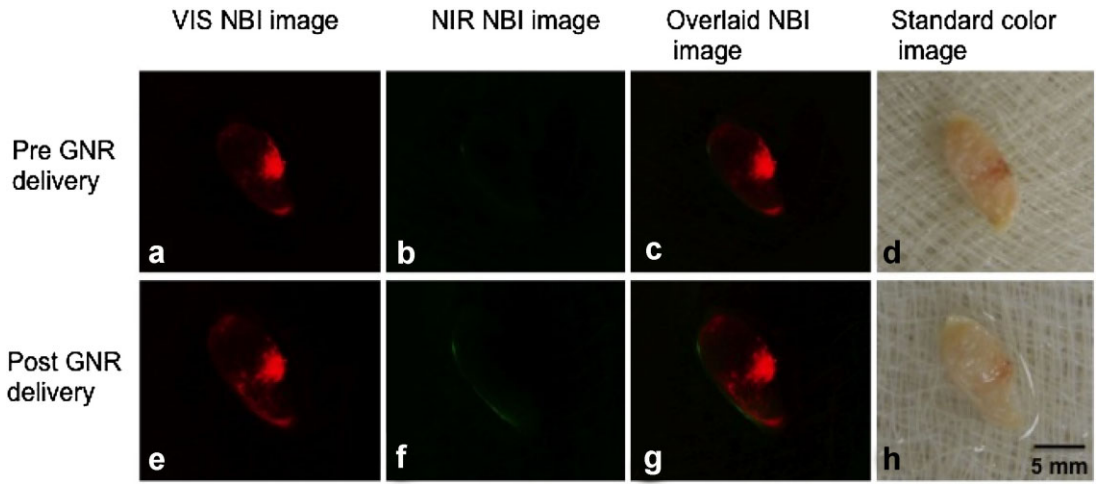

Fig. 3. Images of EGFR over-expressing A431 tumor cross-sections captured before and after the incubation of PEG-GNRs. **a**–**c**: Visible, near-infrared, and overlaid NBI images of A431 tumors before incubation with PEG-GNRs, respectively. **d**: Corresponding standard color image of tumor cross-section. **e**–**g**: Visible, near-infrared, and composite narrow-band imaging images of A431 tumors incubated with PEG-GNRs for 30 minutes at 37°C, respectively. **h**: Corresponding standard color image of tumor cross-section incubated with PEG-GNRs. The red color in the NBI images corresponds to blood. [Color figure can be seen in the online version of this article, available at http://wileyonlinelibrary.com/journal/lsm]

Figure 3, a topical application of PEG-GNRs did not lead to an improvement in image contrast; the mean reflectance intensity was nearly the same as the baseline measure. However, the mean reflectance intensity from tumors treated with C225-GNR was approximately 2.5 times higher than the reflectance from tumors treated with PEG-GNRs ($P < 0.05$) as shown in Figure 5.

Two-Photon Imaging Demonstrating EGFR Binding of C225-GNRs

We performed two-photon microscopy of the tumor samples incubated with both PEG-GNR and C225-GNR to microscopically demonstrate the binding of EGFR targeted GNR in tumors and to study their depth

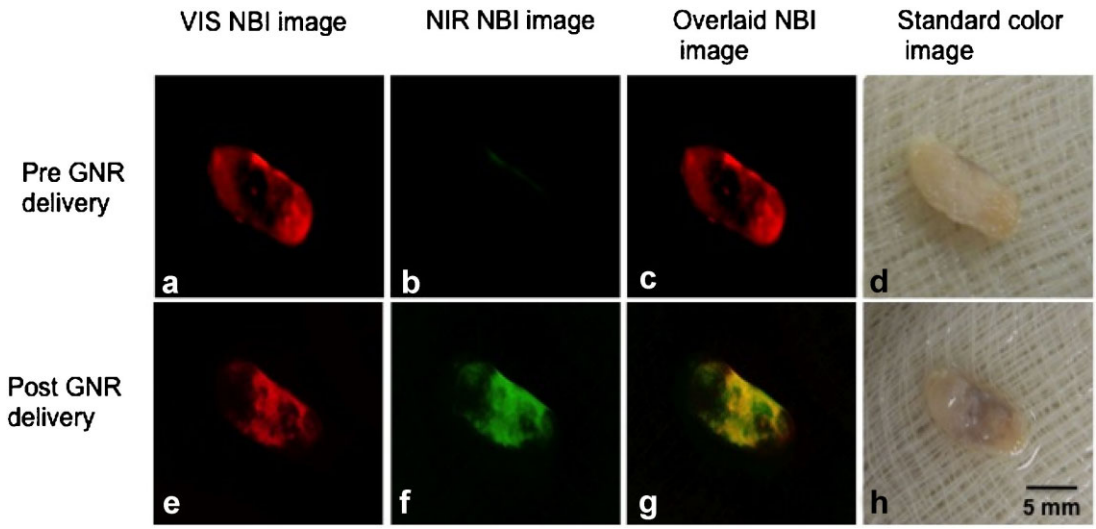

Fig. 4. Images of EGFR over-expressing A431 tumor cross-sections incubated with and without C225-GNRs. **a**–**c**: Visible, NIR, and overlaid NBI images of A431 tumors before incubation with C225-GNRs, respectively. **d**: Corresponding standard color image of tumor cross-section. **e**–**g**: Visible, near-infrared, and composite narrow-band imaging images of A431 tumors incubated with C225-GNRs for 30 minutes at 37°C, respectively. **h**: Corresponding standard color image of tumor cross-section incubated with C225-GNRs. The red color in the NBI images corresponds to blood and the green color corresponds to C225-GNRs attached to EGFRs expressed on A431 tumors. [Color figure can be seen in the online version of this article, available at http://wileyonlinelibrary.com/journal/lsm]

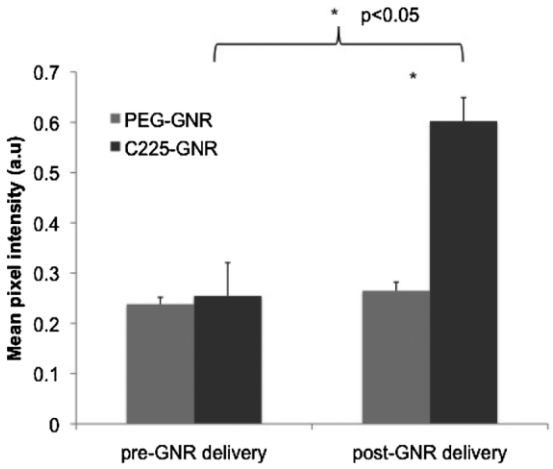

Fig. 5. Mean intensity values for samples of A431 tumors incubated with PEG-GNRs and C225-GNRs. Differences between EGFR over-expressing tumor incubated with PEG conjugated GNRs and EGFR-targeted GNRs was statistically significant ($P < 0.05$, n = 6). Differences between the post and preC225-GNR delivery and incubation was statistically significant ($P < 0.05$, n = 6). Error bars represent standard deviations.

profile. Figure 6a and b represent cross-sectional view of z-projected images of PEG-GNRs and C225-GNRs incubated tumors, respectively. Panels c–f represent *en-face* two-photon images of PEG-GNRs and C225-GNRs-incubated tumors obtained at different depths. C225-GNRs were mostly observed at depths of >100 μm from the tumor surface as seen in Figure 6b. On the other hand, we observed only traces of PEG-GNRs in the control image. A large proportion of signal in the control image can be attributed to instrument noise. This background signal is also visible in the C225-GNR image (Panel f) at 320 μm. The two-photon images of targeted GNR confirmed the specificity of C225-GNRs and their binding affinity to the EGF receptors over expressed in the A431 tumors.

DISCUSSION

In this study, we have shown that anti-EGFR antibody conjugated GNRs combined with near-infrared NBI could yield significant contrast for optical imaging of SCC tumors. We used GNRs conjugated to antibody Cetuximab® (C225) for targeting EGFRs over-expressed in SCC tumors. The antibody conjugation on the GNRs resulted in a 22 nm blue shift in the extinction maximum as seen in Figure 1. The shift in the plasmon resonance peak is possibly due to the change in the local refractive index resulting from antibody conjugation [35]. However, the plasmon peak shift did not hinder imaging of both PEG-GNRs and C225-GNRs due to the optimum bandwidth of the NIR band pass filter utilized.

Topically delivered anti-EGFR antibody conjugated GNRs provided enhanced visualization of A431 tumors using near-infrared NBI. The topical delivery method is a noninvasive approach and can potentially reduce the interaction of particles with untargeted tissues. We have shown that GNRs targeted to EGFR significantly highlight the tumor tissue in the near-infrared NBI image (Fig. 4f) compared to the NBI images of untargeted PEG-GNRs (Fig. 3f). We observed that a small quantity (60 μl) of C225-GNR delivered topically, is sufficient to produce substantial contrast in the images, suggesting that this delivery technique can reduce the amount of nanoparticles required for imaging applications. Recently, Aaron et al. [36] demonstrated molecular binding of topically delivered anti-EGFR gold conjugates on human cervical biopsies and imaged EGFR using reflectance confocal microscopy. Bickford et al. [26] have shown that topically administrated targeted gold nanoshells could help detect HER-2 over-expressing cells in human breast tissue sections using reflectance confocal microscopy. In addition, Nitin et al. [37] evaluated the optical contrast achieved after topical delivery of EGF-Alexa 647 that targeted EGFR in oral lesions using wide-field fluorescence imaging. To our knowledge, we show the first absorption based wide-field optical imaging of anti-EGFR antibody conjugated GNRs targeted to EGFR in SCC tumors. We could potentially combine the effectiveness of the topical delivery method with wide-field NBI to aid in tumor and tumor margin detection during Mohs surgery.

The near-infrared and composite NBI images of tumors incubated with C225-GNRs demonstrated enhanced contrast of the tumors due to the binding of C225 to the EGF receptors. In addition, the comparison of color images and composite NBI images in Figure 4 demonstrated the utility of NIR NBI for better visualization of targeted tumors. We have used gold nanoparticles as contrast agent because they produce localized heating and could cause destruction of cancer cells when irradiated by a NIR laser at their plasmon peak [17]. The NBI platform combined with targeted gold nanorods could potentially guide precise photo-thermal therapy without causing damage to surrounding normal tissue.

Using two-photon microscopy, we evaluated the surface labeling as well as the potential penetration depth of the EGFR-targeted nanorods. Recently, two-photon microscopy has been used to demonstrate effective binding of anti-EGFR GNRs in A431 cells [31] and anti-HER2 gold nanoshells in breast cancer cells [25]. The two-photon images of PEG-GNRs in Figure 6 a, c–f (left columns) demonstrated that there is minimal signal from tumors incubated with untargeted nanoparticles. We observed C225-GNRs at depths >100 μm in the tumors. We believe this large penetration depth could be the result of the long incubation time used in the study. Due to the excellent levels of EGF binding at the current incubation times, we plan to determine the shortest incubation time that can still provide good image contrast. In addition, we plan to conduct studies with EGFR-negative cell lines and a nonspecific control to further confirm the highly specific binding of EGFR-targeted nanorods.

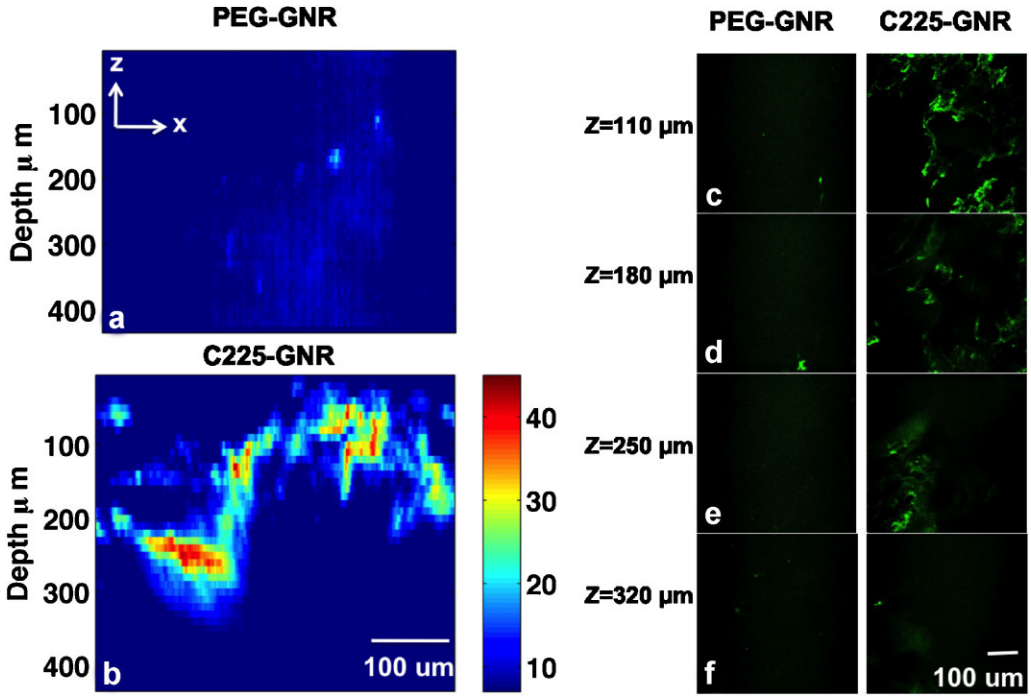

Fig. 6. **a**,**b**: Cross-sectional view of z-projected images of PEG-GNRs and C225-GNRs incubated tumors. **c**–**f**: En-face two-photon images of PEG-GNRs and C225-GNRs accumulated tumors obtained at different depths. C225-GNRs were observed to have maximum accumulation at a depth >100 μm below the tumor surface. a and b are on the same scale. [Color figure can be seen in the online version of this article, available at http://wileyonlinelibrary.com/journal/lsm]

Our results suggest that EGFR could be used as a molecular marker for the assessment of SCC tumors and potentially its margins. Therefore, it is important to understand the distribution of EGF receptors throughout the tumor tissue. We observed a fairly homogenous distribution of the conjugated nanorods on the tumors due to the topical delivery approach. The nanorod distribution is moderately homogenous compared to the accumulation observed with passive tumor targeting of gold nanoparticles shown in previous studies [10]. The tumor microenvironment has vascular abnormalities and poor lymphatics leading to high interstitial fluid pressure [38]. This interstitial hypertension restricts nanoparticle penetration into the tumor core when injected systemically, leading to a heterogeneous distribution in the tumor periphery [39]. However, we believe that the topical delivery approach could help achieve a uniform nanoparticle distribution in tumors. The homogenous distribution of GNRs suggests that this accumulation profile could benefit bulk tumor therapy directed through drugs or photothermal ablation.

CONCLUSION

In summary, topically delivered anti-EGFR antibody conjugated GNRs are effective probes for EGFR expression in SCCs. Using near-infrared NBI and two-photon microscopy, we demonstrated that anti-EGFR GNRs specifically bound to EGFRs over-expressed in A431 tumors and improved optical visualization of SCC tumors. The C225-GNRs attached to the over-expressed EGF receptors providing an enhanced intensity of up to 2.5-fold. Our data suggests that the combined use of targeted nanorods and near-infrared NBI may potentially aid in tumor margin assessment based on EGFR-expression levels serving as a valuable diagnostic tool during surgical resection of SCC tumors.

ACKNOWLEDGMENTS

The authors would like to thank Nanospectra Biosciences Inc. for providing the pegylated gold nanorods. The funding for this research was provided in part by the National Institutes of Health Grant No. R01 CA132032, R21 CA133691, and ASLMS Student Research Grant (2009).

REFERENCES

1. Cancer facts and figures. American Cancer Society. 2009.
2. Rajadhyaksha M, Menaker G, Flotte T, Dwyer PJ, Gonzalez S. Confocal examination of nonmelanoma cancers in thick skin excisions to potentially guide mohs micrographic surgery without frozen histopathology. J Invest Dermatol 2001; 117(5):1137–1143.
3. Yaroslavsky AN, Neel V, Anderson RR. Demarcation of nonmelanoma skin cancer margins in thick excisions using multispectral polarized light imaging. J Invest Dermatol 2003;121(2):259–266.

4. Yaroslavsky AN, Barbosa J, Neel V, DiMarzio C, Anderson RR. Combining multispectral polarized light imaging and confocal microscopy for localization of nonmelanoma skin cancer. J Biomed Opt 2005;10(1):14011.
5. Tannous Z, Torres A, Gonzalez S. In vivo real-time confocal reflectance microscopy: A noninvasive guide for Mohs micrographic surgery facilitated by aluminum chloride, an excellent contrast enhancer. Dermatol Surg 2003;29(8):839–88846.
6. Chung VQ, Dwyer PJ, Nehal KS, Rajadhyaksha M, Menaker GM, Charles C, Jiang SB. Use of ex vivo confocal scanning laser microscopy during Mohs surgery for nonmelanoma skin cancers. Dermatol Surg 2004;30(12):1470–1478.
7. Pierce MC, Strasswimmer J, Park BH, Cense B, de Boer JF. Advances in optical coherence tomography imaging for dermatology. J Invest Dermatol 2004;123(3):458–463.
8. Strasswimmer J, Pierce MC, Park BH, Neel V, de Boer JF. Polarization-sensitive optical coherence tomography of invasive basal cell carcinoma. J Biomed Opt 2004;9(2):292–298.
9. Brancaleon L, Durkin AJ, Tu JH, Menaker G, Fallon JD, Kollias N. In vivo fluorescence spectroscopy of nonmelanoma skin cancer. Photochem Photobiol 2001;73(2):178–183.
10. Puvanakrishnan P, Park J, Diagaradjane P, Schwartz JA, Coleman CL, Gill-Sharp KL, Sang KL, Payne JD, Krishnan S, Tunnell JW. Near-infrared narrow-band imaging of gold/silica nanoshells in tumors. J Biomed Opt 2009;14(2): 024044.
11. Sano Y, Kobayashi M, Hamamoto Y, Kato S, Fu KI, Yoshino T. New diagnostic method based on color imaging using narrow band imaging (NBI) system for gastrointestinal tract. Gastrointest Endosc 2001;53: (5).
12. Muto M, Katada C, Sano Y, Yoshida S. Narrow band imaging: A new diagnostic approach to visualize angiogenesis in superficial neoplasia. Clin Gastroenterol Hepatol 2005; 3(7 Suppl 1):S16–S20.
13. Averitt RD, Westcott SL, Halas NJ. Linear optical properties of gold nanoshells. J Opt Soc Am 1999;16(10):1824–1832.
14. Oldenburg SJ, Averitt RD, Westcott SL, Halas NJ. Nanoengineering of optical resonances. Chem Phys Lett 1998; 288(2–4):243–247.
15. Prodan E, Nordlander P. Structural tunability of the plasmon resonances in metallic nanoshells. Nano Lett 2003;3(4): 543–547.
16. Maeda H, Fang J, Inutsuka T, Kitamoto Y. Vascular permeability enhancement in solid tumor: Various factors, mechanisms involved and its implications. Int Immunopharmacol 2003;3(3):319–328.
17. Goodrich G, Bao L, Gill-Sharp K, Sang K, Wang J, Payne J. Photothermal therapy in a murine colon cancer model using near-infrared absorbing gold nanorods. J Biomed Opt 2010; 15(1):8001–8008.
18. Sokolov K, Follen M, Aaron J, Pavlova I, Malpica A, Lotan R, Richards-Kortum R. Real-time vital optical imaging of precancer using anti-epidermal growth factor receptor antibodies conjugated to gold nanoparticles. Cancer Res 2003;63(9):1999–2004.
19. Loo C, Hirsch L, Lee MH, Chang E, West J, Halas N, Drezek R. Gold nanoshell bioconjugates for molecular imaging in living cells. Optics Lett 2005;30(9):1012–1014.
20. Loo C, Lowery A, Halas N, West J, Drezek R. Immunotargeted nanoshells for integrated cancer imaging and therapy. Nano Lett 2005;5(4):709–711.
21. Huang X, El-Sayed IH, Qian W, El-Sayed MA. Cancer cell imaging and photothermal therapy in the near-infrared region by using gold nanorods. J Am Chem Soc 2006;128(6): 2115–2120.
22. Huang YF, Sefah K, Bamrungsap S, Chang HT, Tan W. Selective photothermal therapy for mixed cancer cells using aptamer-conjugated nanorods. Langmuir 2008;24(20): 11860–11865.
23. James WD, Hirsch LR, West JL, O'Neal PD, Payne JD. Application of INAA to the build-up and clearance of gold nanoshells in clinical studies in mice. J Radioanal Nuclear Chem 2007;271(2):455–459.
24. Nitin N, Carlson AL, Muldoon T, El-Naggar A, Gillenwater A, Richards-Kortum RR. Molecular imaging of glucose uptake in oral neoplasia following topical application of fluorescently labeled deoxy-glucose. Int J Cancer 2009; (124): 2634–2642.
25. Bickford L, Sun J, Fu K, Lewinski N, Nammalvar V, Chang J, Drezek R. Enhanced multi-spectral imaging of live breast cancer cells using immunotargeted gold nanoshells and two-photon excitation microscopy. Nanotechnology 2008; 19(31):315102.
26. Bickford LR, Agollah G, Drezek R. Yu TK. Silica-gold nanoshells as potential intraoperative molecular probes for HER2-overexpression in ex vivo breast tissue using near-infrared reflectance confocal microscopy. Breast Cancer Res Treat 2010;120(3):547–555.
27. Klapper LN, Kirschbaum MH, Sela M, Yarden Y. Biochemical and clinical implications of the ErbB/HER signaling network of growth factor receptors. Adv Cancer Res 2000; 77:25–79.
28. Huang SM, Harari PM. Epidermal growth factor receptor inhibition in cancer therapy: Biology, rationale and preliminary clinical results. Invest New Drugs 1999;17(3):259–269.
29. Maubec E, Duvillard P, Velasco V, Crickx B, Avril MF. Immunohistochemical analysis of EGFR and HER-2 in patients with metastatic squamous cell carcinoma of the skin. Anticancer Res 2005;25(2B):1205–1210.
30. Shimizu T, Izumi H, Oga A, Furumoto H, Murakami T, Ofuji R, Muto M, Sasaki K. Epidermal growth factor receptor overexpression and genetic aberrations in metastatic squamous-cell carcinoma of the skin. Dermatology 2001;202(3):203–206.
31. Durr NJ, Larson T, Smith DK, Korgel BA, Sokolov K, Ben-Yakar A. Two-photon luminescence imaging of cancer cells using molecularly targeted gold nanorods. Nano Lett 2007;7(4):941–945.
32. Melancon MP, Lu W, Yang Z, Zhang R, Cheng Z, Elliot AM, Stafford J, Olson T, Zhang JZ, Li C. In vitro and in vivo targeting of hollow gold nanoshells directed at epidermal growth factor receptor for photothermal ablation therapy. Mol Cancer Ther 2008;7(6):1730–1739.
33. Jana NR, Gearheart L, Murphy CJ. Wet chemical synthesis of high aspect ratio cylindrical gold nanorods. J Phys Chem B 2001;105(19):4065–4067.
34. Park J, Estrada A, Schwartz JA, Diagaradjane P, Krishnan S, Dunn AK, Tunnell JW. Intra-organ biodistribution of gold nanoparticles using intrinsic two-photon induced photoluminescence. Lasers Surg Med; 2010;42(7):630–639.
35. Haes AJ, Stuart DA, Nie S, Van Duyne RP. Using solution-phase nanoparticles, surface-confined nanoparticle arrays and single nanoparticles as biological sensing platforms. J Fluoresc 2004;14(4):355–367.
36. Aaron J, Nitin N, Travis K, Kumar S, Collier T, Park SY, Jose-Yacaman M, Coghlan L, Follen M, Richards-Kortum R, Sokolov K. Plasmon resonance coupling of metal nanoparticles for molecular imaging of carcinogenesis in vivo. J Biomed Opt 2007;12(3): 0340071–0340011.
37. Nitin N, Rosbach KJ, El-Naggar A, Williams M, Gillenwater A, Richards-Kortum RR. Optical molecular imaging of epidermal growth factor receptor expression to improve detection of oral neoplasia. Neoplasia 2009;11(6):542–551.
38. Jain RK, Baxter LT. Mechanisms of heterogeneous distribution of monoclonal antibodies and other macromolecules in tumors: Significance of elevated interstitial pressure. Cancer Res 1988;48(2):7022–7032.
39. Li ML, Schwartz JA, Wang J, Stoica G, Wang LV. In vivo imaging of nanoshell extravasation from solid tumor vasculature by photoacoustic microscopy. SPIE 2007; 64370B.